Robotics and Autonomous Systems 112 (2019) 22–31

Contents lists available at ScienceDirect

Robotics and Autonomous Systems

journal homepage: www.elsevier.com/locate/robot

Improvement of human–machine compatibility of upper-limb rehabilitation exoskeleton using passive joints

Leiyu Zhang [a], Jianfeng Li [b,*], Peng Su [b], Yanming Song [b], Mingjie Dong [a], Qiang Cao [a]

[a] College of Mechanical and Electrical Engineering, Beijing University of Technology, Beijing 100124, China
[b] School of Electromechanical Engineering, Beijing Information Science and Technology University, Beijing 100192, China

HIGHLIGHTS

- Six passive joints were introduced into the connecting interfaces of Co-Exos.
- The optimal configuration can effectively reduce the gravitational influences.
- A new approach is presented to compensate vertical GH movements.
- The passive joints exhibited good human-machine compatibility for GH movements.
- The wearable comfort of Co-Exos was improved significantly.

ARTICLE INFO

Article history:
Received 15 June 2018
Received in revised form 2 September 2018
Accepted 23 October 2018
Available online 9 November 2018

Keywords:
Stroke
Upper-limb rehabilitation exoskeleton
Configuration synthesis
Human-machine compatibility
Passive joint
Glenohumeral joint

ABSTRACT

The upper-limb rehabilitation exoskeleton is a critical piece of equipment for stroke patients to compensate for deficiencies of manual rehabilitation and reduce physical therapists' workloads. In this paper, configuration synthesis of an exoskeleton is completed using advanced mechanism theory. To adapt glenohumeral (GH) movements and improve exoskeletal compatibility, six passive joints were introduced into the connecting interfaces based on optimal configuration principles. The optimal configuration of the passive joints can effectively reduce the gravitational influences of the exoskeleton device and the upper extremities. A compatible exoskeleton (Co-Exos) with 11 degrees of freedom was developed while retaining a compact volume. A new approach is presented to compensate vertical GH movements. The theoretical displacements of translational joints were calculated by the kinematic model of the shoulder loop Θ_s. A comparison of the theoretical and measured results confirms that the passive joints exhibited good human–machine compatibility for GH movements. The hysteresis phenomenon of translational joints appeared in all experiments due to the elasticoplasticity of the upper arm and GH. In comparable experiments, the effective torque of the second active joint was reduced by an average of 41.3% when passive joints were released. The wearable comfort of Co-Exos was thus improved significantly.

1. Introduction

Despite preventive measures, stroke remains a leading cause of permanent disability worldwide [1]. Conventional therapeutic means for functional rehabilitation after stroke have demonstrated limited effectiveness [2], and robotic exoskeletons allow for additional modes of therapy, such as adaptive training and highly repetitive movements [3]. Several groups have developed robotic exoskeletons, such as **CADEN-7** [4], **ARMin** robots [5–7], and **Armeo Power** [8]. Most existing exoskeletons imitate the anatomic structure of the upper limb and connect the upper arm and forearm using straps or woven belts. This kind of exoskeleton is simple, reliable, and sufficiently similar to human joints; however, upper-limb joint kinematics are highly complex and not fully reproducible in rehabilitation exoskeletons, leading to hyperstaticity and human–machine incompatibility [9]. Misalignment between the exoskeleton and glenohumeral joint (GH) also generates constraint forces that reduce the wearable comfort and efficiency of robot-aided training [1,10]. Patients cannot always complete the precise movements they intend during human–robot interactions [3].

To reduce misalignments and improve wearable comfort, a common strategy involves adding active or passive joints to the shoulder actuation of the exoskeleton. For example, two active degrees of freedom (DOFs) in **MEDARM** [11] were installed at the sternoclavicular joint to simulate the shoulder girdle. Nef et al. [5] introduced an active vertical translational joint and two passive joints into **ARMin** to track GH movements. Mihelj et al. [6] added a translational joint in **ARMin II**, which was mechanically coupled

* Corresponding author.
E-mail address: lijianfeng@bjut.edu.cn (J. Li).

https://doi.org/10.1016/j.robot.2018.10.012
0921-8890/

Nomenclature

Θ_s	Shoulder closed-loop
Θ_{ef}	elbow–forearm closed-loop
Θ_{sef}	Human–machine loop
F	DOFs of the spatial multi-loop chain
f_i	DOFs of the ith joint
l	Number of independent loops
d	DOFs of the motion
n	Number of joints
f_k	DOFs of the known joints
f_{uk}	DOFs of the unknown joints
j	Number of known joints
F^s	DOFs of Θ_s
F^{sef}	DOFs of Θ_{sef}
l_s	Number of independent loops in Θ_s
l_{sef}	Number of independent loops in Θ_{sef}
f_k^s	Known DOFs of Θ_s
f_k^{sef}	Known DOFs of Θ_{sef}
f_{uk}^s	Unknown DOFs of Θ_s
f_{uk}^{sef}	Unknown DOFs of Θ_{sef}
f_p^s	Number of passive joints in loops Θ_s
f_p^{ef}	Number of passive joints in loopsΘ_{ef}
R	Passive rotational joint
$\underline{\text{R}}$	Active rotational joints
P	Passive translational joint
M_i	Reference point
$x_0(\phi)$	Displacements of CGH along the axis x_0
$y_0(\phi)$	Displacements of CGH along the axis y_0
$z_0(\phi)$	Displacements of CGH along the axis z_0
φ_{ed}	Elevation/depression inclination
φ_{pr}	Protraction/retraction inclination
ϕ	Elevation angle of the upper limb
α	Included angle α of the elbow joint
d_0	Initial distance
$d_1(\phi)$	Displacements of P_1
$d_2(\phi)$	Displacements of P_2
$d_3(\phi)$	Displacements of P_3
$d_{1,\text{m}}(\phi)$	Measured displacements of P_1
$d_{2,\text{m}}(\phi)$	Measured displacements of P_2
$d_{3,\text{m}}(\phi)$	Measured displacements of P_3
D_1	Moving range of P_1
D_2	Moving range of P_2
D_3	Moving range of P_3
l_{SG}	Length of the vector **SG**
l_0	Initial length of l_{SG}
l_1	Length of ground link o_2o_{g}
l_2	Length of link $o_{\text{g}}o_{\text{R}}$
l_3	Length of link o_2o_{R}

to the elevation angle and mainly compensated for vertical GH movements. Furthermore, the axis of the second joint in **ARMin III** [7] was offset to keep the center of the exoskeleton coincident with that of GH. Based on the design concept of **ARMin III**, **Armeo Power** [8] provided sufficient space at the connection interfaces to compensate for misalignments. Schiele et al. [12] verified the validity of passive joint chains by measuring and analyzing additional constraint forces at the connection interfaces. Schiele [13] then presented a human–machine system with passive joint chains that satisfied kinematic compatibility and did not require alignment to human axes. Grimm et al. [14,15] captured the evolution of movement pattern kinematics of the shoulder and elbow and quantified the individual degree of natural movement restoration for each patient using a multi-joint exoskeleton with seven passive degrees of freedom. Dehez et al. [16] added prismatic and universal joints into the fastening interfaces of **ShouldeRO** to reduce parasitic forces. Vitiello [17] embedded a four-DOF passive mechanism into the elbow exoskeleton, allowing the elbow axis and those of the exoskeleton to be continuously aligned during flex/extension movements. Jarrasse [18] recommended the addition of passive mechanisms inside the mechanism loops to study the general problem of connecting two similar kinematic chains. The exoskeleton of **Dampace** [19] was connected to the global reference frame via a linear guidance system consisting of three perpendicular sliders, each of which could move freely. Two passive mechanisms were introduced into **SUEFUL-7** [20] by considering upper-limb posture and EMG activity levels. Similarly, a passive transitional joint was added into **ASSISTON-SE** [21], which combined with two active transitional joints to reproduce and track the movements of the shoulder girdle. **IntelliArm** [22] adopted a PPP$\underline{\text{R}}$RRR-type serial kinematic chain and utilized two passive joints and an active joint to ensure GH alignment with the device axes.

The aforementioned studies indicate that additional active or passive joints have been adopted in most exoskeleton devices to improve human–machine compatibility. Passive multi-joint exoskeletons may improve stroke rehabilitation exercises by augmentation of feedback with virtual reality and task difficulty adaptation during training [14], closed-loop feedback of movement quality [15], and the application of hybrid solutions with concurrent neuromuscular electrical stimulation [23,24]. Furthermore, active multi-joint exoskeletons have been advanced towards brain–robot interfaces that successfully link three-dimensional robotic training to the participants' efforts and allow for task-oriented practice of activities of daily living with a physiologically controlled multi-joint exoskeleton [25]. Adding passive joints to an actuated exoskeleton can reduce device complexity and improve wearable comfort. As misalignments influence the pose and position of the entire upper limb, prior research contributions have focused mainly on compensations for GH movements while ignoring upper-arm or forearm movements caused by GH.

In this paper, GH, upper limb, forearm, and exoskeleton are taken as a complete human–machine system in configuration synthesis and compatibility analysis of the exoskeleton. An optimal configuration of the upper limb exoskeleton is selected, and a compatible exoskeleton (Co-Exos) with five active joints and six passive joints is developed for upper-limb rehabilitation. This type of configuration can lower the influences of gravity in the exoskeleton device and upper extremities. A new compensation method for GH movements is proposed accordingly. Improvements to the human-machine compatibility of Co-Exos are presented and verified via theoretical analysis and experimental measurement.

2. Design of Co-Exos

Given that GH movements influence the position of the elbow joint, the human-machine system should consist of the entire upper extremity and the exoskeleton device. Based on mechanism theory, kinematic incompatibility of the human-machine system occurs because the chain has insufficient DOFs to accommodate position changes of the GH and elbow joint. Hence, the configuration and DOFs of Co-Exos must be synthesized and analyzed before finalizing the structural design.

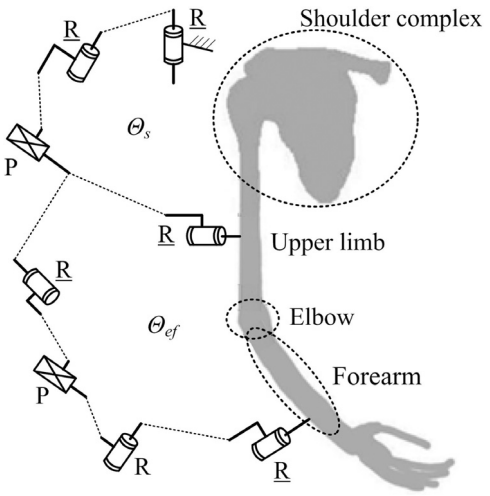

Fig. 1. Schematic diagram of human-machine system.

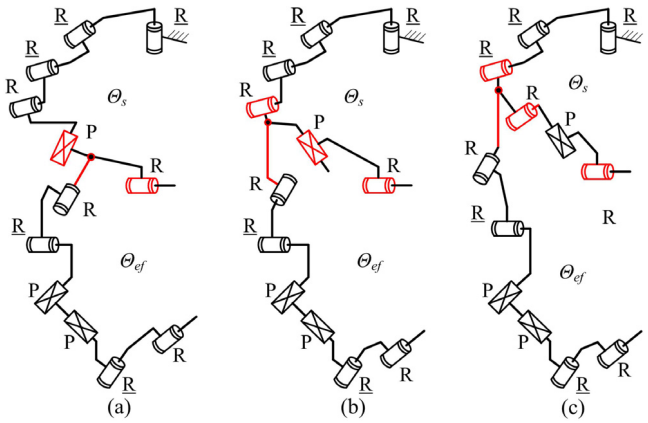

Fig. 2. Combination of 3R2RP and 2R2R2P.

Table 1
Configurations of two sub-chains ($f_p^s = 4, f_p^{ef} = 3$).

Sub-chain	Number of active joints	Number of passive joints	Configuration
Shoulder sub-chain	3	4	3R4R, 3R3RP, 3R2R2P, 3RR3P
elbow–forearm sub-chain	2	3	2R3R, 2R2RP, 2RR2P, 2R3P

2.1. Configuration synthesis of upper-limb exoskeleton

Upper-limb exoskeleton devices include five active rotational joints to realize motor functions: ab/adduction, flex/extension, in/external rotations of GH, flex/extension of the elbow, and in/external rotation of the forearm [26]. The human–machine system is a spatial multi-loop chain composed of a shoulder closed loop Θ_s and an elbow–forearm closed loop Θ_{ef} as shown in Fig. 1. All active or passive joints of the exoskeletons are limited to a single-DOF rotation or prismatic joint, denoted as R and P, respectively. According to mechanism theory, the DOFs of the spatial multi-loop chain, F, can be calculated using Hunt's formula [18,27], which is expressed as

$$F = \sum_{i=1}^{n} f_i - d \cdot l \tag{1}$$

where f_i denotes the DOFs of the ith joint, l is the number of independent loops, d denotes the DOFs of the motion with which a mechanism is intended to function (for the spatial chain, $d = 6$), and n is the number of joints.

To ensure clear understanding of the distribution of active or passive joints, Formula (1) can be translated into the following expression:

$$F = f_k + f_{uk} - d \cdot l \tag{2}$$

where f_k and f_{uk} denote DOFs of the known and unknown joint, respectively; and j is the number of known joints.

Based on the configuration of active joints in general exoskeletons, the DOFs of Θ_s and the human-machine loop Θ_{sef} (respectively denoted as F_s and F_{sef}) can be determined, where $F_s = 3$ and $F_{sef} = 5$. Similarly, the number of independent loops in Θ_s and Θ_{sef}, denoted as l_s and l_{sef} are known such that $l_s = 1$ and $l_{sef} = 2$. For the closed-loop Θ_s, three active joints exist in the exoskeleton, and three biological DOFs are in the shoulder; hence, f_k^s denotes the known DOFs of Θ_s where $f_k^s = 6$. The known DOFs of Θ_{sef} are denoted as f_k^{sef} where $f_k^{sef} = 10$. Based on these parameters, the unknown DOFs of loops Θ_s and Θ_{sef}, denoted as f_{uk}^s and f_{uk}^{sef}, can be obtained by

$$f_{uk}^s = F_s + d \cdot l_s - f_k^s = 3 + 6 - 6 = 3 \tag{3}$$

$$f_{uk}^{sef} = F_{sef} + d \cdot l_{sef} - f_k^{sef} = 5 + 12 - 10 = 7 \tag{4}$$

Eqs. (3) and (4) indicate that loop Θ_s, as an independent loop, needs at least three passive DOFs. Seven DOFs should be added to loop Θ_{sef}. If five or more DOFs are introduced into an independent loop, then the passive joint chain becomes too long, and the efficiency of power and driving forces declines sharply [1]. Hence, only two combinations of passive joints are applied in loops Θ_s and Θ_{ef} as follows:

$$f_p^s = 3,\ f_p^{ef} = 4;\ f_p^s = 4,\ f_p^{ef} = 3$$

where f_p^s and f_p^{ef} denote the number of passive joint in loops Θ_s and Θ_{ef}, respectively.

To simplify the joint structures, only single-DOF joints R or P are introduced into the shoulder sub-chain and elbow–forearm sub-chain of the exoskeleton. To distinguish active and passive rotational joints, R is used to denote the active joint. The two sub-chains each have four configurations when $f_p^s = 4$, $f_p^{ef} = 3$ as shown in Table 1. The configurations are enumerated in Table 2 when $f_p^s = 3$, $f_p^{ef} = 4$. When ignoring the connecting position and sequence of the passive joints, the exoskeleton mechanism possesses 32 configurations for the above two combinations; otherwise, the combination of 3R2RP and 2R2R2P (Table 2) has at least three exoskeleton configurations as shown in Fig. 2. The only difference among the configurations in Fig. 2 is the connecting position between the two sub-chains.

As seen in the configuration synthesis of the exoskeleton mechanism, many possible configurations exist. Selecting suitable configurations that possess engineering value is difficult. Hence, referring to the active joint distributions of mature rehabilitation exoskeletons, namely **Armin III** [7], **Armeo Power** [8], and **CADEN-7** [4], the optimal configuration principles are as follows:

(1) Active joints should be distributed along the upper-limb skeleton.

(2) Influences on the exoskeleton's gravity on active joints and the upper limb should be reduced as much as possible.

(3) The length of the sub-chains should be as short as possible to improve the efficiency of driving forces.

(4) Preferentially use prismatic joint P.

The combination of 3RR3P and 2R2RP (Table 1) was selected for this study according to the optimal principles. By calculating and

Table 2
Configurations of two sub-chains ($f_p^s = 3, f_p^{ef} = 4$).

Sub-chain	Number of active joints	Number of passive joints	Configuration
Shoulder sub-chain	3	3	3R3R, 3R3P, **3R2RP**, 3RR2P
elbow–forearm sub-chain	2	4	2R4R, 2R3RP, **2R2R2P**, 2RR3P

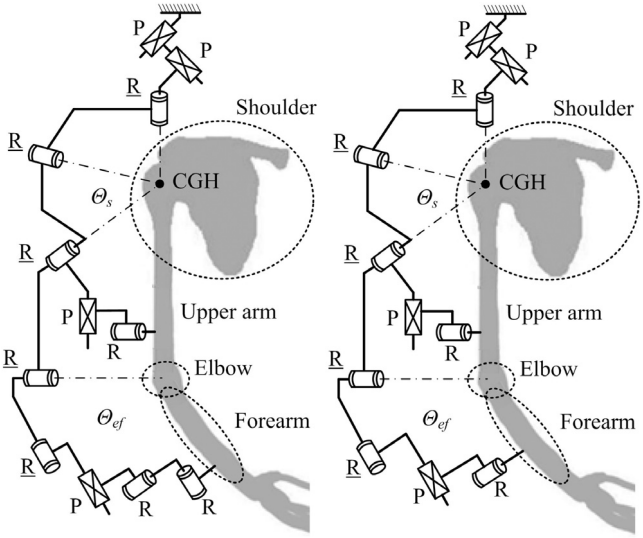

(a) 2P3RPR and 2RP2R ($f_p^s = 4, f_p^{ef} = 3$) (b) 2P3RPR and 2RPR ($f_p^s = 4, f_p^{ef} = 2$)

Fig. 3. Configurations of exoskeleton mechanism.

comparing the dexterity and manipulability under different specific configurations, an optimal configuration was determined as illustrated in Fig. 3a. The shoulder sub-chain 2P3RPR was deemed the best configuration of 3RR3P considering the connecting position and sequence. In the exo-skeleton, the first joint R is installed vertically and the axes of the three joints R converge to the center of GH (CGH). Additionally, two joints P are installed horizontally at the front section with another joint P along the upper arm. The passive joint R connects the third joint P and the upper arm. This configuration of the shoulder sub-chain can lower the influence of gravity for the exoskeleton device and upper extremities.

Similarly, the elbow–forearm sub-chain 2RP2R was chosen as the configuration of 2RP2R (Fig. 3a). Joint P is fixed at the second active joint R and connected to the remaining joints R. The last joints R are arranged serially. In the sub-chain 2RP2R, the in/external rotation of the forearm is driven by the second joint R; the passive sub-chain P2R is situated between that joint R and the forearm. To reduce the complexity of this sub-chain and improve transmission efficiency, the sub-chain 2RP2R can be simplified as 2RPR as depicted in Fig. 3b. Hence, two identical passive sub-chains PR are installed at the connection interfaces of the upper arm and forearm. Given the above configuration synthesis, the sub-chains 2P3RPR and 2RPR are employed in this paper as a compatible configuration of the upper-limb exoskeleton.

2.2. Structural design of Co-Exos

The structure of Co-Exos was designed in detail according to the compatible configuration. The Co-Exos prototype consists of an adjustable turntable, a cantilever, and a main exoskeleton mechanism as pictured in Fig. 4. The entire exoskeleton was mounted

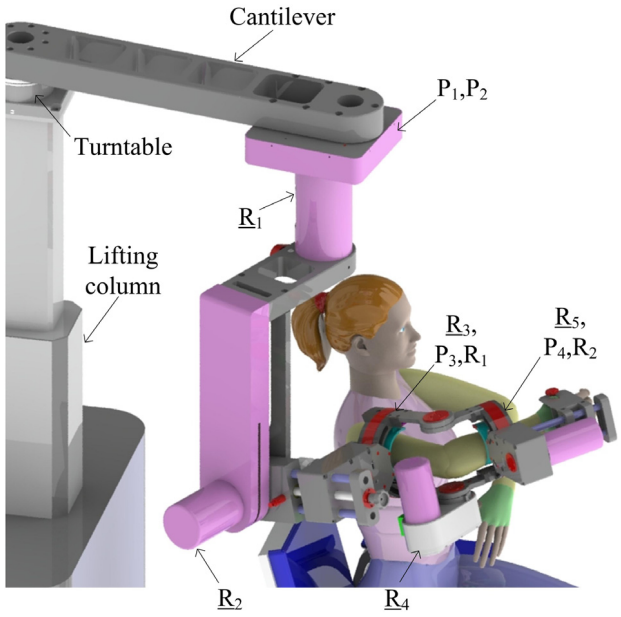

Fig. 4. Structure of Co-Exos.

onto an actuated lifting column to adjust for different heights. The main exoskeleton mechanism was installed below the front of the cantilever that rotated around the turntable within a specific range to fit with different shoulder widths. Co-Exos was applied for right-arm use in the configuration shown in Fig. 4, although the device can be easily switched from right-arm to left-arm use.

The five active rotational joints, denoted by R_1, R_2, R_3, R_4, and R_5, were arranged serially. The DC-motor power in joint R_1 was transmitted to the output shaft through an HD gearbox (1:80). A torque sensor (M2210G; SRI Inc., China) was mounted between the gearbox and the shaft to monitor the output torque. An absolute angular encoder (AksIM; RLS Inc., Slovenia) was fixed on the other terminal of the output shaft to measure the positions of R_1; R_2 and R_4 had a similar structure as R_1. The output of the HD gearbox (1:50) in R_4 was connected to the elbow joint via a belt drive (1:1) to avoid colliding with the human body. R_3 and R_5 followed a similar drive principle with additional components as shown in Fig. 5. The power of R_3 and R_5 was transmitted to the outer semi-circle via another belt drive (1:4). The belt drives consisted of a synchronous pulley, synchronous belt, and guide pulleys. The outer semi-circle was driven and rotated along the supporting rollers. The difference between R_3 and R_5 was that the volume and radius of the outer and inner semi-circles in R_3 were more significant than those in R_5. The detailed actuation is shown in Table 3.

Joints P_1 and P_2 were vertically fixed through a combination of double linear guides and sliders as shown in Fig. 6a. Joint P_2 was installed under the moving plate of P_1. To improve support for the main exoskeleton and upper extremities, two extension springs were introduced into each translational joint. The active joint R_1 was connected with the bottom of P_2. The passive joints P_3 and R_1 were mounted in the outer semi-circle of R_3 (Fig. 5). P_3 adopted a combination of dual mini linear guides and sliders. The two linear guides were fixed inside the outer semi-circle. The inner semi-circle could move freely along the axis of the outer circle as shown in Fig. 6b. Joint R_1 was fixed inside the inner semi-circle and connected to the upper arm by the semi-ring and the woven belt. Two compressed springs were installed at both sides of each slider. Passive joints P_4 and R_2 had a similar configuration and structure as P_3 and R_1, respectively. The passive joints can improve the human–machine compatibility of Co-Exos, and constraint forces resulting from misalignments decline substantially.

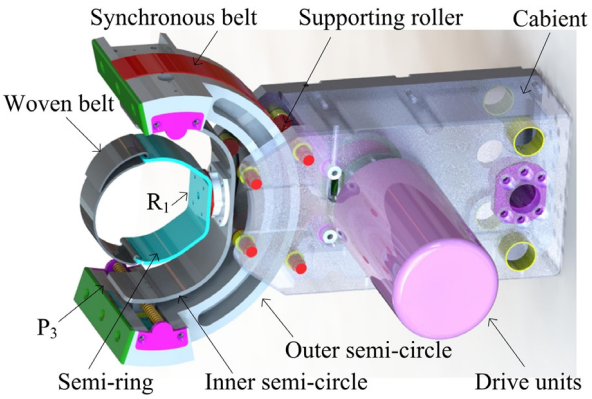

Fig. 5. Active joints $\underline{R_3}$.

Table 3
Actuation of Co-Exos.

Active joint	Gearbox	Motor type
R_1: Angle plane of elevation	Harmonic Drive[a] 1:80	Kollmorgen TBM 76 Brushless DC[b]
R_2: Arm elevation	Harmonic Drive[a] 1:120	Kollmorgen TBM 76 Brushless DC[b]
R_3: In/external shoulder rotation	Harmonic Drive[a] 1:30+ Belt Drive 1:4	Kollmorgen TBM 60 Brushless DC[b]
R_4: Flex/extension of elbow	Harmonic Drive[a] 1:50+ Belt Drive 1:1	Kollmorgen TBM 60 Brushless DC[b]
R_5: In/external forearm rotation	Harmonic Drive[a] 1:30+ Belt Drive 1:4	Kollmorgen TBM 60 Brushless DC[b]

[a]Harmonic Drive Inc., Japan
[b]Kollmorgen Inc., America

Based on the compatible configuration and detailed structure, a Co-Exos prototype was developed as shown in Fig. 7. Two adjustable units were introduced into the exoskeleton to fit different lengths of the upper arm or forearm. Co-Exos is mainly applied to patients with upper-limb dyskinesia caused by stokes or spinal cord injuries. According to the muscle strength levels, three rehabilitation modes are provided for the whole upper limb: passive, active and resistance modes.

3. Kinematic models of passive joints

This paper proposes a new compensation method for GH movements. Kinematic models of passive joints were established based on the kinematics of GH to clarify the relevant movements in the elevation process.

3.1. Kinematic model of GH

The GH joint of the shoulder complex has a ball-and-socket structure. As the GH position varies with the posture of the upper limb, it is difficult to keep the exoskeleton axes in alignment with human axes in real time. Previous experiments and measurements [28,29] have sought to identify kinematic characteristics of GH in healthy humans. Klopcar et al. [28] fastened reference points M_1–M_{11} onto the anterior and posterior region of the shoulder girdle as shown in Fig. 8. The motions of all reference points were captured and measured with an Optotark system in the four anatomical planes (front plane 0°, plane 45°, sagittal plane 90°, and plane 135°). Mathematical expressions of GH movements were deduced

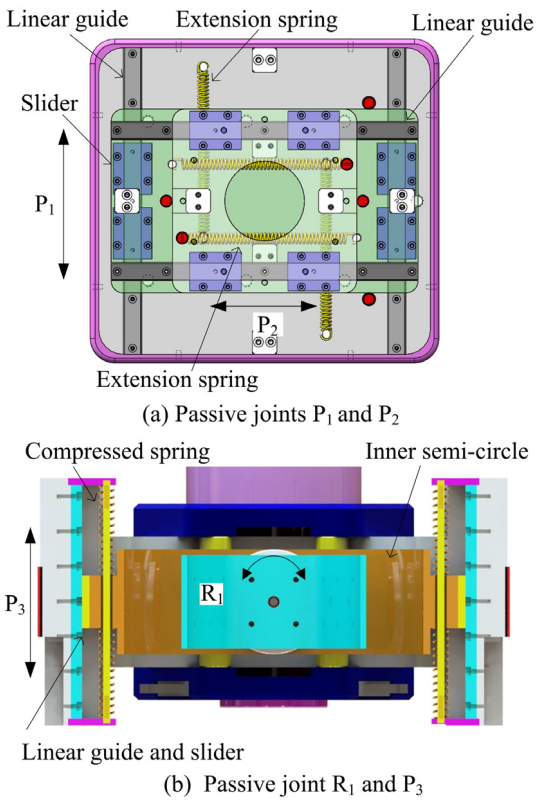

Fig. 6. Passive joints.

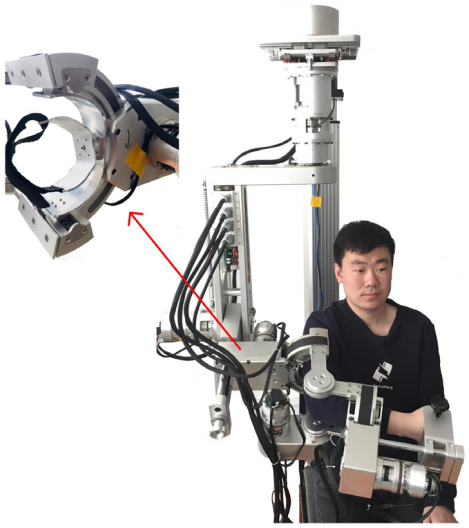

Fig. 7. Co-Exos prototype.

based on the measured results. The origin o_0 of the reference coordinate {0} is at the intersection of the medial–lateral axis through CGH and the anterior–posterior axis through the sterna. The vector SG points from the calculated point S (center of M_3 and M_5) to point G (center of M_4 and M_6). The displacements of CGH along three directions in the coordinate {0} can be obtained by the following equations:

$$\begin{cases} x_0(\phi) = l_{SG} \cdot \cos\phi_{ed} \cdot \cos\phi_{pr} \\ y_0(\phi) = l_{SG} \cdot \cos\phi_{ed} \cdot \sin\phi_{pr} \\ z_0(\phi) = l_{SG} \cdot \sin\phi_{ed} \end{cases} \tag{5}$$

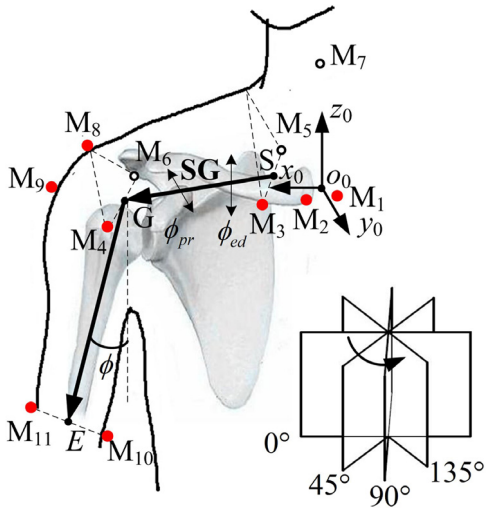

Fig. 8. Reference points on shoulder complex.

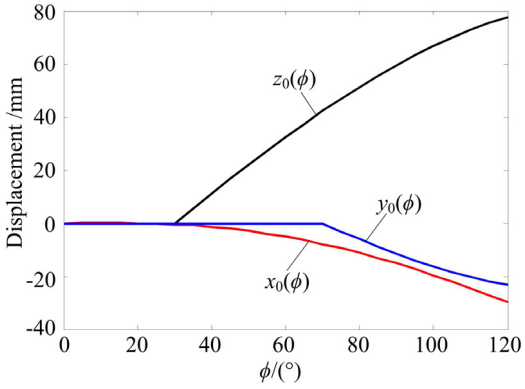

Fig. 9. CGH displacements.

where l_{SG} denotes the length of the vector **SG**, φ_{ed} is the elevation/depression inclination, φ_{pr} is the protraction/ retraction inclination, and ϕ is the elevation angle of the upper limb. The three parameters (l_{SG}, φ_{ed}, φ_{pr}) are the correlation functions of the elevation angle ϕ,

$$l_{SG} = (-1.6 \times 10^{-5}\phi + 3 \times 10^{-4}\phi + 1) \cdot l_0$$

$$\phi_{ed} = \begin{cases} -0.3\phi & \phi < 0° \\ 0 & 0° \le \phi \le 30° \\ 0.36\phi - 10.8° & \phi > 30° \end{cases}$$

$$\phi_{pr} = \begin{cases} 0.35\phi & \phi < 0° \\ 0 & 0° \le \phi \le 70° \\ -0.22\phi + 15.4° & \phi > 70° \end{cases}$$

where l_0 denotes the initial length of l_{SG}.

A group of 20 healthy Chinese individuals (average height = 177 cm and average weight = 72 kg) participated in the experiment to measure the reference point coordinates using a VICON system (Oxford Metrics Inc., UK). The l_0 lengths of the participants were calculated at an average length of l_0 = 180 mm. Hence, the displacements $x_0(\phi)$, $y_0(\phi)$, and $z_0(\phi)$ were calculated as $0° < \phi < 120°$ as shown in Fig. 9. The vertical GH movements have the greatest range of motion. The compensation for $z_0(\phi)$ was analyzed emphatically in this section.

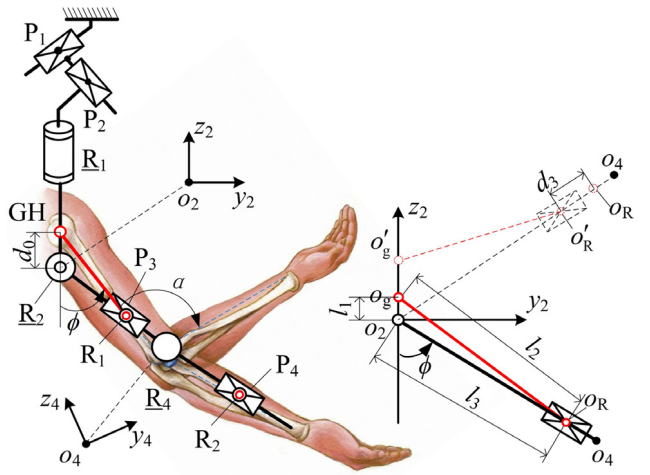

(a) Shoulder closed loop Θ_s (b) Simplified mechanism of Θ_s

Fig. 10. Shoulder closed loop Θ_s.

3.2. Kinematic model of loop Θ_s

Joints P_1, P_2, and P_3 in the loop Θ_s were used to track the aforementioned GH displacements. The configuration analysis of Θ_s reveals that the moving plane of P_3 included an angle relative to that of P_1 or P_2. Hence, the movements of P_3 exhibited a weak coupling relationship with those of P_1 and P_2. The relationship was also indeterminable due to the friction and spring force of passive joints. To reduce this coupling relationship, the stiffness of springs in P_1 and P_2 was designed to be higher than that in P_3. Joints P_1 and P_2 were distributed to adjust $x_0(\phi)$ and $y_0(\phi)$ of CGH; therefore, the displacements of P_1 and P_2 in the coordinate $x_c o_c y_c$, denoted by $d_1(\phi)$ and $d_2(\phi)$, can be obtained such that

$$\begin{cases} d_1(\phi) = x_0(\phi) = l_{SG} \cdot \cos\phi_{ed} \cdot \cos\phi_{pr} \\ d_2(\phi) = y_0(\phi) = l_{SG} \cdot \cos\phi_{ed} \cdot \sin\phi_{pr} \end{cases} \tag{6}$$

The upper arm was connected to the semi-ring of R_1 by woven belts. Joint R_1 was mounted inside the translational joint P_3 to move along the axis of $\underline{R}_3$. A coordinate system {2} was fixed on the center of $\underline{R}_2$, and its three axes were parallel to those of {0}. The loop Θ_s consisted of the shoulder sub-chain 2P3$\underline{R}$PR and the upper arm. To understand the kinematics of Θ_s during the elevation process, the loop Θ_s was projected onto the plane $y_2 o_2 z_2$, as shown in Fig. 10a. In this paper, a new approach is proposed to compensate the vertical displacements $z_0(\phi)$. The main mechanism of Co-Exos was offset along the axis z_0 by the lifting column. Joint $\underline{R}_2$ was placed above GH at the initial distance d_0. The human–machine system, including joints $\underline{R}_3$, P_3, R_1, and GH, can be simplified as a guide-bar mechanism as shown in Fig. 10b. $o_2 o_g$, $o_2 o_4$, and $o_g o_R$ denote the ground link, grounded link, and upper arm, respectively; o_g, o_4, and o_R denote the centers of GH, $\underline{R}_4$, and R_1. As an input link, $o_2 o_4$ rotates around the center o_2. The upper limb $o_g o_R$ is elevated by the link $o_2 o_4$, and the point o_g moves upwards. Hence, the length l_1 of the ground link $o_2 o_g$ varies with the elevation angle ϕ. The dashed line in Fig. 10b indicates a configuration of the guide-bar mechanism during the elevation process. The length l_1 and angle ϕ influence length l_3 of link $o_2 o_R$. Additionally, the change of length l_3 is the theoretical displacement $d_3(\phi)$ of joint P_3. Using the trigonometric function, the length $l_3(\phi)$ can be deduced:

$$l_3(\phi) = l_1 \cdot \cos\phi + \sqrt{l_2^2 - l_1^2 \cdot \sin 2\phi} \tag{7}$$

where l_2 denotes the length of the link $o_g o_R$, $l_1(\phi) = d_0 - z_0(\phi)$.

Table 4
Main parameters of Co-Exos.

Parameter	Value	Parameter	Value
d_0/mm	30	D_1/mm	−50–50
l_2/mm	150	D_2/mm	−50–50
l_3/mm	271.5	D_3,/mm	0–120

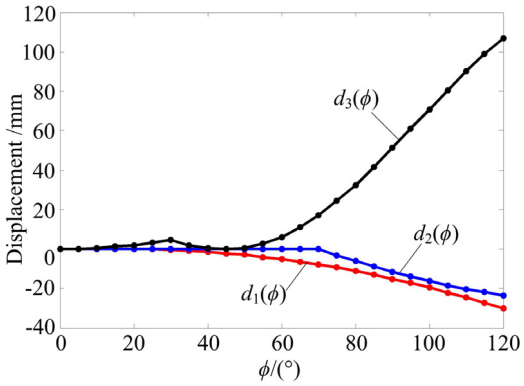

Fig. 11. Displacements of passive joints.

Then, the displacement $d_3(\phi)$ can be obtained by the following expression:

$$d_3(\phi) = l_3(\phi_0) - l_3(\phi) \tag{8}$$

where ϕ_0 denotes the initial elevation angle.

The main parameters of Co-Exos are listed in Table 4, where D_1, D_2, and D_3 respectively denote the moving range of P_1, P_2, and P_3. The theoretical displacements of GH can be calculated through the established kinematic model shown in Fig. 11. The displacement $d_3(\phi)$ increases nearly linearly with an increase in the elevation angle ϕ. The maximum $d_{3,\max}$ of $d_3(\phi)$ is equal to 106 mm.

4. Experimental system of Co-Exos

The purpose of this experiment was to evaluate the compensation for GH and wearable comfort by measuring the displacements of passive joints and torques of active joints during the elevation process. Three draw-wire displacement sensors (WFS1000; Fiaye Inc., China) were used to measure the displacements of P_1, P_2, and P_3, respectively, as shown in Fig. 12a. The sensor frame was glued on the linear guide using hot melt adhesives, and the free end of the wire rope was connected to the slider. The measured displacements of P_1, P_2, and P_3 are denoted by $d_{1,\mathrm{m}}(\phi)$, $d_{2,\mathrm{m}}(\phi)$, and $d_{3,\mathrm{m}}(\phi)$.

As mentioned in Section 2.2, five torque sensors (M2210G; SRI Inc., China) were added in each active joint to detect and observe the output torques. The torque sensors were used to measure and evaluate the constraint forces between the upper limb and exoskeleton device. The upper arm and forearm were connected to passive joints R_1 and R_2. The constraint forces were transmitted to active joints $\underline{R}_3$ and $\underline{R}_5$ as shown in Fig. 12b. The coordinate systems {2}, {3}, and {5} were fixed on the virtual centers of $\underline{R}_2$, $\underline{R}_3$, and $\underline{R}_5$, respectively. The upper arm applied friction F_f^3 and pressing forces F_x^3 and F_z^3 on joint $\underline{R}_3$. These three forces were parallel to the three axes of {3}. Similarly, the forearm applied the constraint forces F_f^5, F_x^5, and F_z^5 on joint $\underline{R}_5$. These six forces were found to influence wearable comfort and should therefore be reduced as much as possible. The constraint forces produced torques at joint $\underline{R}_1$, $\underline{R}_2$, and $\underline{R}_4$. Constraint forces were thus acquired indirectly by measuring the output torques of $\underline{R}_1$, $\underline{R}_2$, and $\underline{R}_4$, denoted by T_1, T_2, and T_4, respectively. As the passive joints could be locked and released, the improvement in human-machine compatibility of Co-Exos could be evaluated by comparing the output torques under the locked and released conditions.

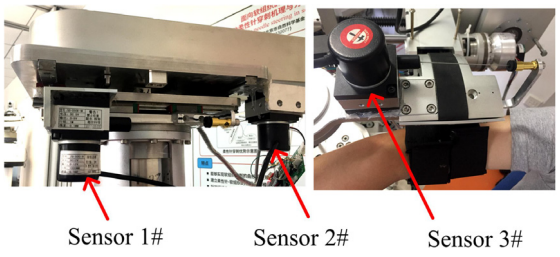

(a) Draw-wire displacement sensors

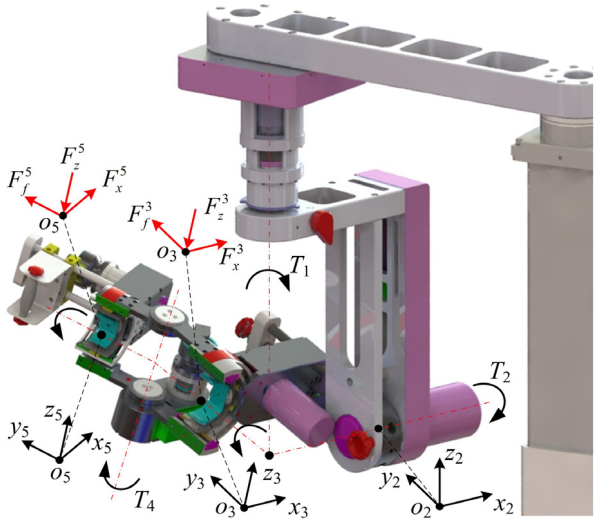

(b) Schematic diagram of constraint forces

Fig. 12. Experimental system of Co-Exos.

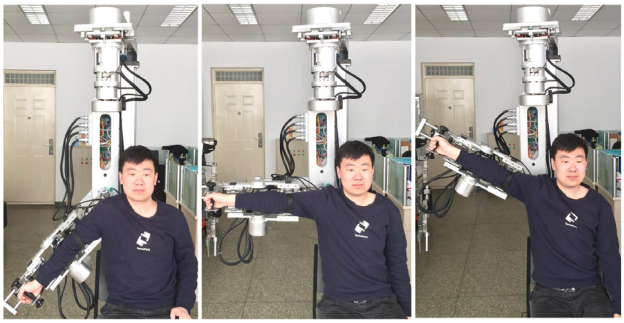

Fig. 13. Elevation experiments.

For the stroke patients, the movements of GH and upper limb are weaker and stiffer due to muscle atrophy or lost of physiological muscles synergies. Additionally, they are not sensitive to constraining forces. Hence, the group of 20 healthy volunteers mentioned above participated in the experiments to verify the technical specifications of Co-Exos and the compensation methods for GH movements. The right upper limb of each individual was connected to the inner semi-cycle of P_3 or P_4 by woven belts. Based on the experimental system, a detailed scheme of the elevation experiment was formulated. The main exoskeleton was elevated by the distance d_0 relative to the initial position of GH ($\phi = 0°$). The following experiments were conducted. **(I)** Experiment to verify

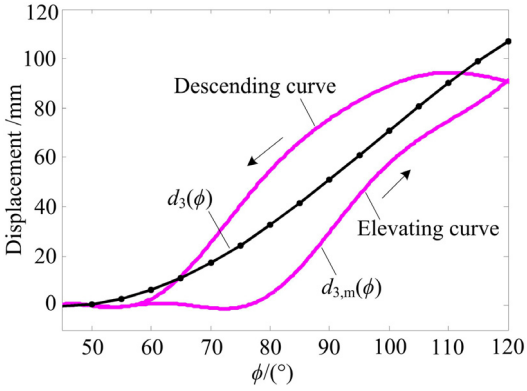

Fig. 14. Displacements $d_{3,m}(\phi)$ in Experiment I.

the simplified mechanism: only the upper limb was connected with passive joint R_1; joints P_1 and P_2 were locked. **(II)** Compatible experiment of loop Θ_s: only the upper arm was bounded with the exoskeleton and elevated under the anatomical planes 0°, 45°, and 90°; all passive joints were released. **(III)** Compatible experiment of loops Θ_s and Θ_{ef}: the upper arm and forearm were each connected to the exoskeleton, and the upper limb was elevated at the anatomical plane 0°, as shown in Fig. 13; the upper limb was elevated at different elbow angles α (Fig. 10). **(IV)** Experiment without passive joints: the entire upper limb wore Co-Exos, and all passive joints were locked. As the passive joints barely moved at $\phi = 0°$–45° (Fig. 11), the upper limb was elevated from 45° to 120° in the above experiments.

5. Results and discussion

As the participants have different body sizes, the measured displacements used in this section are the mean values in each experiment. In Experiment I, only passive joint P_3 was released. The kinematics of P_3 could be observed clearly in the elevating and descending processes. Fig. 14 displays the measured displacements $d_{3,m}(\phi)$ at the 90° anatomical plane. The maximum of $d_{3,m}(\phi)$ and $d_3(\phi)$ was 95 mm and 105 mm, respectively. The displacements $d_{3,m}(\phi)$ had a similar range and shape compared with those of $d_3(\phi)$ in the elevation process. The joint P_3 tracked GH movements approximately at $\phi = 45°$–120°. Additionally, joint P_3 exhibited a nonlinear path and significant hysteresis. During the elevation process, P_3 remained stationary at $\phi = 45°$–80° and moved quickly at $\phi = 80°$–120°. Meanwhile, the descending curve of $d_{3,m}(\phi)$ lagged and did not duplicate the trajectory of the elevation curve, presumably due to elasticoplasticity in the connecting upper arm and GH.

In Experiment II, joints P_1, P_2, and P_3 were released and corresponding displacements were measured at elevation planes of 0°, 45°, and 90°, as shown in Fig. 15. The variation ranges of $d_{1,m}(\phi)$ and $d_{2,m}(\phi)$ were consistent with those of $d_1(\phi)$ and $d_2(\phi)$. The kinematics of P_1 and P_2 had a certain correlation with the elevation planes; the moving planes of P_1 and P_2were parallel to the 0° and 90° elevation plane, respectively. Results show that the smaller the acute angle between the moving plane and the elevation plane, the more intensive its influence on joint P_1 or P_2. Joint P_3 of loop Θ_s exhibited similar kinematic characteristics under the different elevation planes. The hysteresis phenomenon still existed in the sliding process of P_3. Joint P_3 could mostly compensate the vertical GH movements; hence, the Co-Exos prototype in Experiment II could accommodate GH movements by passive joints.

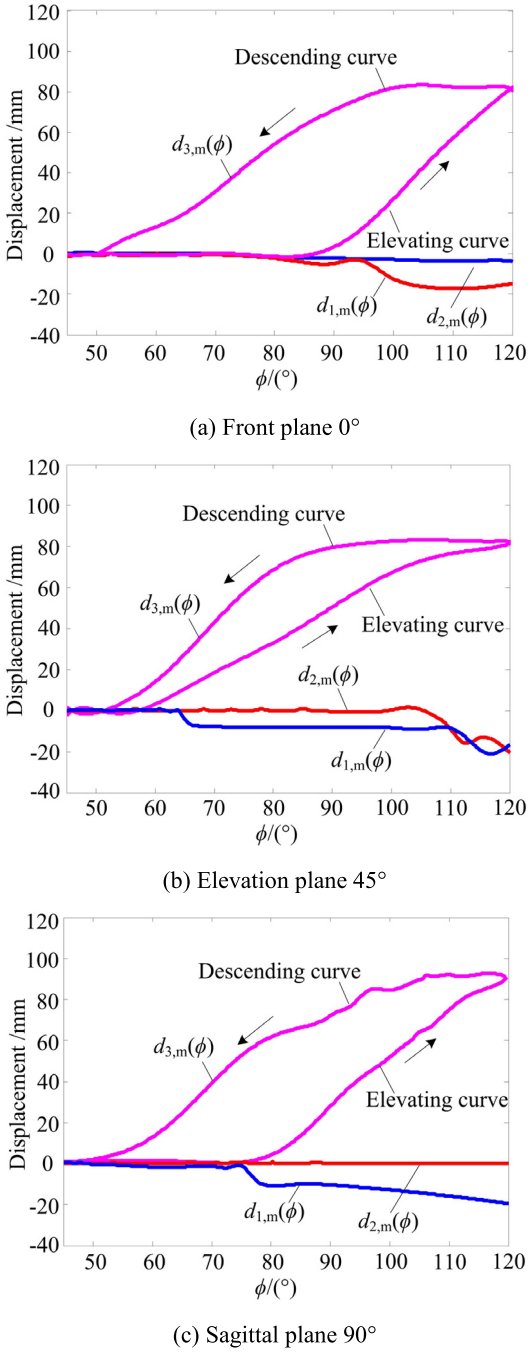

Fig. 15. Measured displacements of passive joints in loop Θ_s.

Experiment III, the human–machine compatibility experiment, was implemented at the 90° elevation plane to analyze the influences of the elbow angle α. As joints P_1 and P_2 had similar kinematic characteristics in this experiment, associated discussions are omitted here. The elbow angle α exerted a great influence on the joint P_3, as shown in Fig. 16. The sliding range of P_3 declined, and the relevant hysteresis increased with a decrease in α. The kinematic stability declined during the elevating and descending processes due to additional forces. The passive joints could make up for more than half the GH movements. When the passive joints did not compensate the GH movements, participants adjusted their posture to fit and reduce constraint forces at the connection interfaces. As loop Θ_{ef} is an under-constraint loop, the human–machine chain consisting of Θ_s and Θ_{ef} is an under-constraint loop

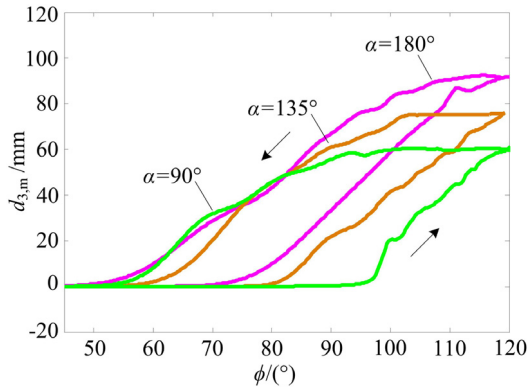

Fig. 16. Displacements $d_{3,m}(\phi)$ in Experiment III.

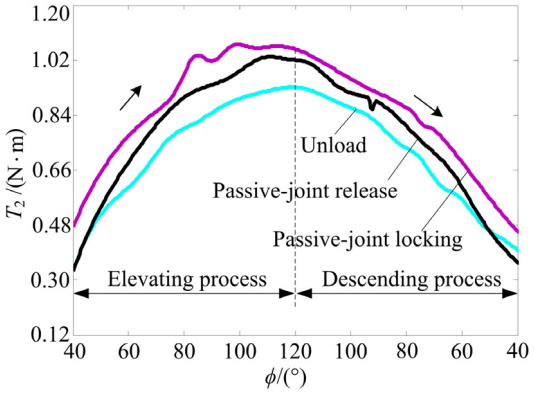

Fig. 17. Torque T_2 at the 90° elevation plane.

when α is less than 180°. Human–machine compatibility for the entire upper limb declined slightly compared with the first two experiments.

In Experiment IV, three experiments were completed for unloading, passive-joint release, and passive-joint locking at the 90° elevation plane and $\alpha = 180°$. During the elevation process, GH movements had little influence on active joints $\underline{R}_1$, $\underline{R}_3$, and $\underline{R}_4$, and the corresponding torques changed slightly. The torque T_2 of $\underline{R}_2$ was a focal point as depicted in Fig. 17. The three curves of T_2 exhibited a similar shape during the elevating and descending processes. An approximate balance system was added in joint $\underline{R}_2$, and the unload torque T_2 remained at a lower level. When the entire extremity wore the exoskeleton and all passive joints were locked, the torque T_2 increased along the unload curve. The differences between the torques with and without the upper limb denoted the effective drive torque of $\underline{R}_2$. When the passive joints were released, the effective torque declined by an average of 41.3%. The constraint forces in the connection interfaces were positively correlated to the effective torque. Hence, the wearable comfort of Co-Exos was improved substantially. Human–machine incompatibility due to insufficient DOFs can apparently be alleviated by adding six passive joints to the prototype.

6. Conclusions

(1) To adapt GH movements and improve the compatibility of upper-limb exoskeletons, six passive joints were introduced into the connecting interfaces of Co-Exos based on configuration synthesis and optimal configuration principles. The optimal configuration of the passive joints could effectively reduce gravitational influences of the exoskeleton device and the upper extremities. The Co-Exos prototype with 11 DOFs still possessed a compact structure and volume.

(2) A new approach is presented here to compensate vertical GH movements. The theoretical displacements of translational joints were calculated using the kinematic model of shoulder loop Θ_s. The passive joints exhibited good compensations for GH movements based on comparison of the theoretical and measured results. Additionally, the hysteresis phenomenon in the translational joints existed in all experiments due to the elasticoplasticity of the upper arm and GH.

(3) In compatible experiments, the effective torque of $\underline{R}_2$ was reduced by an average of 41.3% when passive joints were released. The constraint forces in the connection interfaces showed a positive relationship with the effective torque; hence, the wearable comfort of Co-Exos was notably improved.

Acknowledgments

This research is partially supported by the projects of National Natural Science Foundation of China (No. 51705007, No. 51675008), Natural Science Foundation of Beijing Municipality (No. 3171001, No. 17L20019), Natural Science Foundation of Beijing Education Committee (No. KM201810005015) and China Postdoctoral Science Foundation (2018T110017).

References

[1] V. Klamroth-Marganska, J. Blanco, K. Campen, et al., Three-dimensional, task-specific robot therapy of the arm after stroke: a multicentre, parallel-group randomised trial, Lancet Neurol. 13 (2) (2014) 159–166.
[2] R.P. Van Peppen, G. Kwakkel, S. Wooddauphinee, et al., The impact of physical therapy on functional outcomes after stroke: what's the evidence? Clin. Rehabil. 18 (8) (2004) 833.
[3] N. Jarrassé, T. Proietti, V. Crocher, et al., Robotic exoskeletons: a perspective for the rehabilitation of arm coordination in stroke patients, Front. Hum. Neurosci. 8 (947) (2014) 1845–1846.
[4] J.C. Perry, J.M. Powell, J. Rosen, Isotropy of an upper limb exoskeleton and the kinematics and dynamics of the human arm, Appl. Bionics Biomech. 6 (2) (2009) 175–191.
[5] T. Nef, M. Mihelj, R. Riener, ARMin: a robot for patient cooperative arm therapy, Med. Biol. Eng. Comput. 45 (9) (2007) 887–900.
[6] P. Staubli, T. Nef, V. Klamrothmarganska, Robert Riener, Effects of intensive arm training with the rehabilitation robot ARMin II in chronic stroke patients: four single-cases, J. NeuroEng. Rehabil. 6 (1) (2009) 46.
[7] T. Nef, M. Guidali, R. Riener, ARMin III - arm therapy exoskeleton with an ergonomic shoulder actuation, Appl. Bionics Biomech. 6 (2) (2009) 127–142.
[8] V. Klamrothmarganska, J. Blanco, K. Campen, et al., Three-dimensional, task-specific robot therapy of the arm after stroke: a multicentre, parallel-group randomisedtrial, Lancet Neurol. 13 (2) (2014) 159–166.
[9] H.C. Crockett, L.B. Gross, K.E. Wilk, et al., Osseous adaptation and range of motion at the glenohumeral joint in professional baseball pitchers., Am. J. Sports Med. 30 (1) (2002) 20–26.
[10] N. Jarrasse, M. Tagliabue, J.V.G. Robertson, et al., A methodology to quantify alterations in human upper limb movement during Co-manipulation with an exoskeleton, IEEE Trans. Neural Syst. Rehabil. Eng. 18 (4) (2010) 389.
[11] S.J. Ball, I.E. Brown, S.H. Scott, MEDARM: a rehabilitation robot with 5 DOF at the shoulder complex, in: IEEE/ASME International Conference on Advanced Intelligent Mechatronics, Piscataway, USA, 2007, pp. 124–129.
[12] A. Schiele, An explicit model to predict and interpret constraint force creation in pHRI with exoskeletons, in: 2008 IEEE International Conference on Robotics and Automation, Pasadena, USA, 2008, pp. 1324–1330.
[13] A. Schiele, G. Hirzinger, A new generation of ergonomic exoskeletons: the high-performance X-Arm-2 for space robotics telepresence, in: 2011 IEEE/RSJ International Conference on Intelligent Robots and Systems, Pasadena, USA, 2011, pp. 2158–2163.
[14] F. Grimm, G. Naros, A. Gharabaghi, Closed-loop task difficulty adaptation during virtual reality reach-to-grasp training assisted with an exoskeleton for stroke rehabilitation, Front. Neurosci. 10 (518) (2016) 1–13.
[15] F. Grimm, G. Naros, A. Gharabaghi, Compensation or restoration: Closed-loop feedback of movement quality for assisted reach-to-grasp exercises with a multi-joint arm exoskeleton, Front. Neurosci. 10 (280) (2016) 1–8.
[16] B. Dehez, Sapin, O. Jpse. ShouldeR, ShouldeRO, an alignment-free two-DOF rehabilitation robot for the shoulder complex, in: 2011 IEEE International Conference on Rehabilitation Robotics, Zurich, Switzerland, 2011, pp. 1–6.

[17] N. Vitiello, T. Lenzi, S. Roccella, et al., NEUROExos: a powered elbow exoskeleton for physical rehabilitation, IEEE Trans. Robot. 29 (1) (2013) 220–235.
[18] N. Jarrasse, G. Morel, Connecting a human limb to an exoskeleton, IEEE Trans. Robot. 28 (3) (2013) 697–709.
[19] A.H.A. Stienen, E.E.G. Hekman, G.B. Prange, et al., Stienen AHA Hekman EEG Prange GB others Dampace: design of an exoskeleton for force-coordination training in upper-extremity rehabilitation, J. Med. Dev. Trans. ASME 3 (3) (2009) 031003.1-031003.10.
[20] K. Kiguchi, M.H. Rahman, M. Sasaki, et al., Development of a 3-DOF mobile exoskeleton robot for human upper-limb motion assist, Robot. Auton. Syst. 56 (8) (2008) 678–691.
[21] M. Yalcin, V. Patoglu, Kinematics and design of AssistOn-SE: A self-adjusting shoulder-elbow exoskeleton, in: IEEE Ras & Embs International Conference on Biomedical Robotics and Biomechatronics, IEEE, 2012, pp. 1579–1585.
[22] H.S. Park, Y. Ren, L.Q. Zhang, IntelliArm: An exoskeleton for diagnosis and treatment of patients with neurological impairments, in: IEEE Ras & Embs International Conference on Biomedical Robotics and Biomechatronics, IEEE, 2008, pp. 109–114.
[23] G. Florian, W. Armin, S. Martin, et al., Hybrid neuroprosthesis for the upper limb: Combining brain-controlled neuromuscular stimulation with a multi-Joint arm exoskeleton:, Front. Neurosci. 10 (367) (2016) 1–11.
[24] F. Grimm, A. Gharabaghi, Closed-loop neuroprosthesis for reach-to-grasp assistance: Combining adaptive multi-channel neuromuscular stimulation with a multi-joint arm exoskeleton, Front. Neurosci. 10 (284) (2016) 1–13.
[25] B. Daniel, V. Mathias, B. Robert, et al., Brain state-dependent robotic reaching movement with a multi-joint arm exoskeleton: combining brain-machine interfacing and robotic rehabilitation, Front. Hum. Neurosci. 9 (564) (2015) 1–13.
[26] Han Jianyou, Advanced Mechanisms, China Machine Press, Beijing, 2004, pp. 15–25.
[27] Y. Fang, L.W. Tsai, Enumeration of a class of over constrained mechanisms using the theory of reciprocal screws, Mech. Mach. Theory 39 (11) (2004) 1175–1187.
[28] N. Klopcar, J. Lenarcic, Bilateral and unilateral shoulder girdle kinematics during humeral elevation, Clin. Biomech. 21 (1) (2006) 20–26.
[29] B. Ugurlu, M. Nishimura, K. Hyodo, et al., Proof of concept for robot-aided upper limb rehabilitation using disturbance observers, IEEE Trans. Hum.-Mach. Syst. 45 (1) (2015) 110–118.

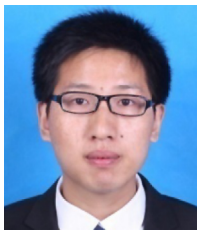

Leiyu Zhang received M.S. (2009) and PhD (2016) in mechanical engineering in Beihang Univ., China. He is now a lecturer at the College of Mechanical and Electrical Engineering at the Beijing Univ. of Technology. His work focuses on rehabilitation exoskeletons, configuration analysis, physical Human–Robot interaction, interaction control and movement analysis.

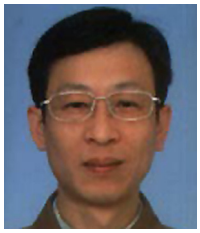

Jianfeng Li received PhD in mechanical engineering (1999) in Beihang Univ., China. After a postdoctor at Tsinghua Univ., he came back to Beijing Univ. of Technology in 2001 and was elected as a professor in 2014. Over these years, his research interests focuses on theory of mechanism, rehabilitation exoskeletons, robotic and wearable devices.